Spin distribution of the compound nucleus in heavy ion reactions at near-barrier energies

S. Gil,* R. Vandenbosch, A. J. Lazzarini, D.-K. Lock, and A. Ray
University of Washington, Seattle, Washington 98195
(Received 21 December 1984)

Gamma ray multiplicities and the (HI,xn) cross sections for the dominant reaction channel were measured at near-barrier bombarding energies for the systems $\alpha+{}^{154}$Sm and ^{12}C+^{154}Sm. The mean value of the spin distribution of the compound nucleus was obtained for each of the systems studied. The results of these measurements together with the results of an earlier study on ^{16}O+^{154}Sm indicate that at bombarding energies near and below the Coulomb barrier the spin distributions of the compound nucleus are broader than the triangular distributions expected from a sharp cutoff model, these deviations being larger for the more massive projectiles. The different behavior of the three systems clearly indicates the importance of the centrifugal barrier penetrability in determining the spin distribution of the compound nucleus. The absolute values of the mean angular momentum can be accounted for if one also includes deformation effects. A one-dimensional barrier-penetration model including the effect of averaging over the orientation of the deformed target can account for the experimental results.

I. INTRODUCTION

The quantum mechanical barrier penetration effects play a central role in near- and sub-barrier fusion reactions, since classically one expects the fusion cross section to vanish suddenly as the bombarding energy becomes less than the interaction barrier. Barrier penetration and reflection not only affect the dependence of the fusion cross section at near- and sub-barrier energies, but also the distribution of strength for the different partial waves which are crucial in determining the spin distribution of the compound nucleus (CN). There is increasing evidence that some features of sub-barrier fusion cross sections cannot be explained in terms of a quantum mechanical treatment of a one-dimensional barrier, and that the coupling of additional degrees of freedom has to be considered. Such couplings can result in fluctuations in the effective barrier height for each partial wave. We will concentrate our attention in this work on the understanding of the spin distribution of the compound nucleus at near-barrier energies, and its connection with centrifugal barrier fluctuations and penetrabilities.

There are a number of reasons that make the study of the spin distribution an interesting subject. It is well known that the branching ratios for γ ray, neutron, proton, alpha particle, and fission decay of the CN are very sensitive to the angular momentum of the CN.[1,2] The relative yields of xn and $(x+1)n$ evaporation products are also quite sensitive to the width of the spin distribution.[3] Also the angular distribution of fission fragments in fusion-fission reactions depends on the spin distribution of the CN.[2] There have been several recent reports of anomalous moments of inertia deduced from fission fragment angular distributions which may reflect spin distribution effects.[4,5] It would be useful to have reliable ways of predicting the spin distribution of the compound nucleus produced in fusion reactions, as well as simple physical pictures of the relevant parameters that determine this distribution.

The spin distribution of the CN has often been parametrized using the sharp cutoff model, where only the partial waves l, below a certain value $l_{\rm crit}$, are assumed to contribute to the fusion cross section and with probability equal to one. This assumption becomes progressively worse as the reduced mass of the entrance channel increases, as well as when the bombarding energy decreases toward the barrier energy.

In a recent publication,[2] we reported on a study of the compound nucleus spin distribution for the ^{16}O+^{154}Sm system. We deduced from this measurement a fairly broad spin distribution of the CN at near-barrier energies. The mean spin values could be reproduced by calculations which incorporated both centrifugal barrier penetration effects and target deformation effects. In order to isolate the effect of the centrifugal barrier penetrability on the spin distribution of the CN, in the present work we have performed similar experiments on the same target using different projectiles so as to vary the reduced mass of the entrance channel, while maintaining the target deformation constant.

The effective potential $V_{\rm eff}(r,l)$ for the entrance channel can be written as the sum of nuclear, Coulomb, and centrifugal potentials. At the effective interaction distance R_b, where $V_{\rm eff}$ reaches its maximum, we have

$$V_{\rm eff}(R_b,l)=V_b+\frac{l(l+1)\hbar^2}{2\mu R_b^2} \tag{1}$$

in the usual notation, where l is the orbital angular momentum in the entrance channel, μ is the effective inertia parameter, and V_b is the Coulomb barrier resulting from the sum of the nuclear and Coulomb potentials. We see that the magnitude of μR_b^2 strongly affects the contribution of the centrifugal potential to the effective interac-

tion barrier for each partial wave. Consequently by studying the dependence of the spin distribution of the CN for systems with different reduced masses, we can address the question of how relevant the centrifugal potential is in determining these spin distributions. We have therefore extended our previous study of the $^{16}O+^{154}Sm$ system to the $\alpha+^{154}Sm$ and $^{12}C+^{154}Sm$ systems. According to preliminary statistical decay model calculations using the code CASCADE (Ref. 6), the main channel open at near-barrier energies for the last two systems are the $(\alpha,2n)$ and $(^{12}C,4n)$, respectively. The residual nuclei produced by these reactions are well deformed even-even nuclei with known gamma-decay schemes.[7]

The method for characterizing the spin distribution of the CN that was available to us consisted in determining the first two moments of this distribution, proportional to the moment of order 0, σ_{fus}, and the moment of order 1, $\langle l \rangle$. The fusion cross section was determined from the measurement of the channel cross section (HI,xn), σ_{xn}, where x corresponds to the main decay channel of the CN, and a statistical model calculation of the (smaller) yields of unobserved channels. The channel cross section was determined from the γ-ray yield associated with the γ decay of the residual nucleus produced in the reaction (HI,xn). The average angular momentum was determined from gamma-ray multiplicity measurements.

II. EXPERIMENT

The experimental method used for determining the gamma-ray multiplicities M_γ and the channel cross sections σ_{xn} is the same as was used in Ref. 2. The experimental setup consisted of two 7.6×7.6 cm NaI detectors placed at 55° and 125° with respect to the beam, and a 26.9% efficient Ge(Li) detector placed at 90° with respect to the beam, 4 cm from the target. An example of the singles and coincidence gamma ray spectra taken with the Ge(Li) detector is shown in Fig. 1. A silicon surface barrier detector was placed at 30° as a monitor for obtaining absolute cross sections.

A self-supporting enriched ^{154}Sm (98.7%) target of 500 $\mu g/cm^2$ was used. All the beam energies were corrected to the midpoint of the target.

III. EXPERIMENTAL RESULTS

A. Gamma-ray multiplicities and average angular momenta

The γ multiplicities were determined from the ratio of the intensities of a given γ transition in the Ge(Li) spectrum in coincidence with any γ ray in either of the NaI detectors to the intensity of the same transition in the singles Ge(Li) spectrum. The results are given in Tables I and II.

We follow a procedure similar to the one we have used previously[2] for converting M_γ into $\langle l \rangle$. The relationship we use is

$$\langle l \rangle = 1.65(M_\gamma - 2.4) , \tag{2}$$

which is consistent with the expressions employed by other authors[8,9] for nuclei in the same region of the periodic table. It is based on measured multiplicities for reactions

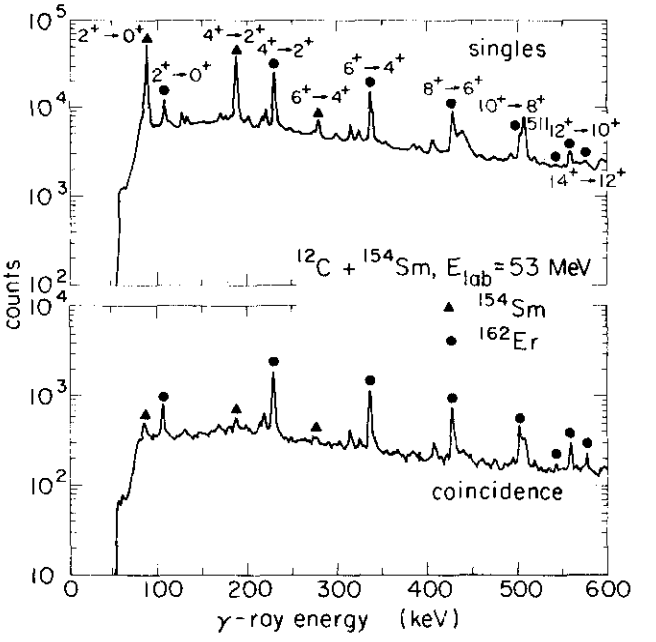

FIG. 1. Singles and coincidence Ge(Li) spectra for the reaction $^{12}C+^{154}Sm$ at $E_L=53$ MeV. A dot on top of a peak indicates a transition in ^{162}Er, whereas a triangle indicates a gamma transition in ^{154}Sm.

where the input angular momentum is relatively well understood.[10] It has an asymptotic behavior for $\langle l \rangle \to 0$ of $M_\gamma = 2.4$ that is compatible with the $M_\gamma \simeq 4 \pm 1$ observed in thermal neutron capture reactions, where the average angular momentum brought to the CN is nearly zero. [In the case of (HI,xn) reactions, the average excitation energy leading to gamma emission is half the neutron binding energy for low $\langle l \rangle$, whereas in the case of the thermal neutron capture reaction, the excitation energy is the neutron binding energy.]

In order to estimate the absolute uncertainty in using Eq. (2), we follow a technique similar to the one that we have used previously,[2] namely, we consider two extreme possibilities that are still compatible with the calibration reaction data for the dependence of M_γ on $\langle l \rangle$ in this region of the periodic table. These are dependencies of the same general form as Eq. (2), but with different slopes,

$$l_1 = 1.82(M_\gamma - 3.3) \tag{3}$$

and

$$l_2 = 1.51(M_\gamma - 1.5) . \tag{4}$$

B. Channel cross sections σ_{xn}

We have used the singles Ge(Li) spectra together with the information obtained from the monitor for determining the transition cross section $\sigma_{xn}(J)$, i.e., the cross section for the transition $J \to J-2$ in the residual nucleus produced after the emission of x neutrons. The channel cross section σ_{xn}, for each bombarding energy, was determined by extrapolating the transition cross section to $J=0$. We fit the measured transition cross sections as a function of the parent spin J using the empirical expression

TABLE I. Measured $4^+ \rightarrow 2^+$ transition cross sections $\sigma(\alpha,2n)$ and their uncertainties $\Delta\sigma$, total fusion cross sections σ_{fus} and their total absolute uncertainties $\Delta\sigma_{fus}$, rotational cascade intensity distribution parameters J_0 and C [Eq. (5)], using $a=1.6$, gamma ray multiplicities M_γ and their uncertainties ΔM_γ, and mean angular momenta $\langle I \rangle$ [Eq. (2)] for the $\alpha+{}^{154}$Sm reaction. (Note the following: In Tables I and II, the values of $\Delta\sigma$ include only the statistical uncertainties, whereas the values of $\Delta\sigma_{fus}$ include the uncertainties due to statistics and accuracy in the determination of σ_{fus}, as well as an estimated uncertainty of 8% in the calculated yields. All these contributions were added in quadrature.)

E_{lab} (MeV)	$\sigma(\alpha,2n)$ (mb)	$\Delta\sigma$ (mb)	σ_{fus} (mb)	$\Delta\sigma_{fus}$ (mb)	J_0	C (mb)	M_γ	ΔM_γ	$\langle I \rangle$
15	8	4	18	9	2.7	9.5	2.8	0.7	0.7
15.5	23	4	48	5	2.9	26	2.8	0.3	0.7
16	41	3	82	9	3.5	45.6	3.1	0.25	1.2
16.5	80	5	145	14	3.7	87	3.3	0.5	1.5
17	139	8.3	224	22	3.7	152	3.7	0.2	2.1
17	148	8	238	24	3.7	163	3.8	0.2	2.3
17.5	219	13	313	30	3.9	239	4.1	0.2	2.8
18	317	19	423	42	4.1	341	4.4	0.2	3.3
19	506	30	595	60	4.2	543	5.0	0.2	4.3
20	552	35	600	60	5.0	576	5.7	0.2	5.4
20	672	40	730	73	5.0	703	5.5	0.2	5.1
21	698	42	735	73	5.5	721	6.0	0.15	5.9
21	730	44	768	77	5.5	754	6.0	0.15	5.9
22	874	55	920	65	6.1	822	6.5	0.15	6.8
22	796	48	838	84	6.1	809	6.5	0.15	6.8
23	807	48	867	86	6.3	823	7.0	0.2	7.6
24	907	54	1008	100	6.5	890	7.4	0.2	8.2
24	875	55	972	97	6.2	894	7.3	0.2	8.1

$$Y(J)=C/\{1+\exp[(J_0-J)/a]\} \ . \tag{5}$$

The channel cross section is then given by $\sigma_{xn} \equiv Y(J=0)$. The parameters J_0, C, and a were varied so as to minimize the χ^2 fit to the data at each bombarding energy. For each of the systems studied we found that a constant value of the width parameter a gave a reasonable fit at all bombarding energies. For the case of ^{154}Sm$(\alpha,2n)$ we used $a=1.6$, and for the case of ^{154}Sm$(^{12}C,4n)$ we used $a=3.5$. Examples of transition cross sections and their fits are given in Fig. 2. We also noticed a smooth increase of J_0 with the bombarding energy for each of the reactions studied (see Tables I and II). We have previously shown that this procedure gives channel cross sections for $^{16}O+{}^{154}$Sm in good agreement with the results obtained by Stokstad *et al.*[11] by a different method.

With regard to other decay channels [e.g., $(x-1)n$, $(x+1)n$] that may be open at certain bombarding energies for each system, we have not been able to determine their cross section. In the singles Ge(Li) spectra it has not been possible to identify any lines that would be associated with the γ transitions among the known low-lying states in the corresponding residual nuclei. The reason for not seeing these lines may be associated with the fact that

TABLE II. Measured $4^+ \rightarrow 2^+$ transition cross sections $\sigma(^{12}C,4n)$ and their statistical uncertainties $\Delta\sigma$, total fusion cross sections σ_{fus} and their total absolute uncertainties $\Delta\sigma_{fus}$, rotational cascade intensity distribution parameters J_0 and C [Eq. (5)] using $a=3.5$, gamma-ray multiplicities M_γ and their uncertainties ΔM_γ, and mean angular momenta $\langle I \rangle$ [Eq. (2)] for the $^{12}C+{}^{154}$Sm reaction.

E_{lab} (MeV)	$\sigma(^{12}C,4n)$ (mb)	$\Delta\sigma$ (mb)	σ_{fus} (mb)	$\Delta\sigma_{fus}$ (mb)	J_0	C (mb)	M_γ	ΔM_γ	$\langle L \rangle$
46.7	1.7	0.5	8	4	2.0	2.7	4.9	0.6	4.1
47.7	5.8	0.8	22	4.2	2.0	9.1	4.8	1.0	4.0
48.7	16.3	1.5	51	8.6	2.5	24	5.3	1.1	4.8
49.7	40.3	2.5	89	16	3.0	57	6.2	0.6	6.3
49.7	42	3	93	12	3.0	61	5.9	0.6	5.8
50.7	82	5	150	15	3.5	112	6.9	0.4	7.4
51.7	123	6	199	20	4.0	163	7.0	0.4	7.6
52.7	177	11	263	26	4.5	229	7.9	0.3	9.1
54.7	271	17	361	36	5.5	327	8.7	0.3	10.4
56.7	323	20	409	36	6.5	373	10.1	0.3	12.7
58.7	411	26	514	51	7.5	459	11.1	0.3	14.4
60.7	414	26	545	54	8.5	451	11.4	0.3	14.9

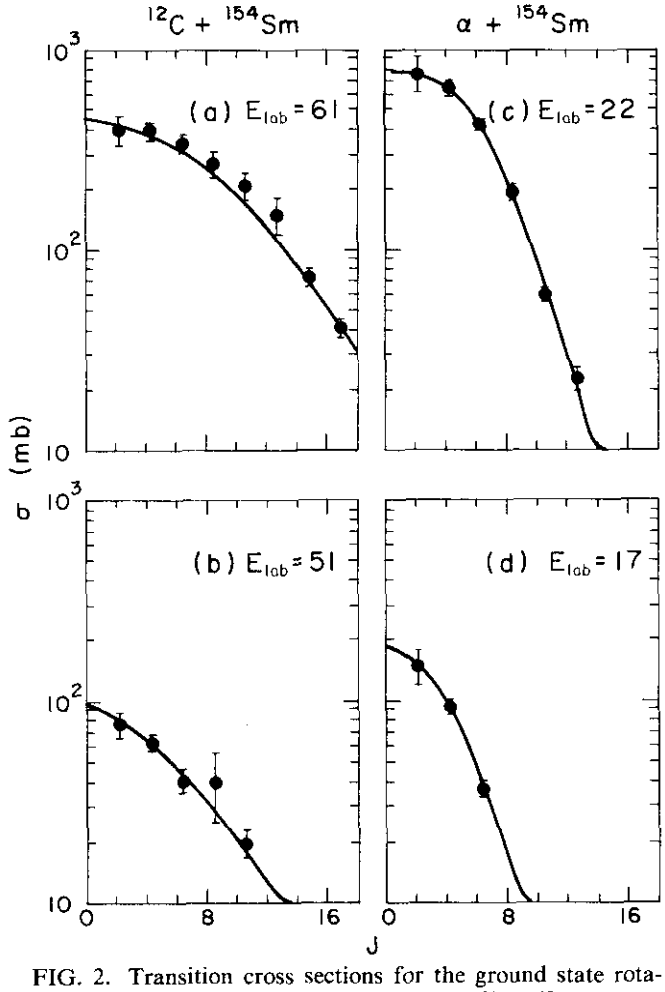

FIG. 2. Transition cross sections for the ground state rotational band transition J-J-2 produced in the $^{154}Sm(^{12}C,4n)$ (left panels) and the $^{154}Sm(^{4}He,2n)$ (right panels) reactions. The full curves are Fermi function fits to the data as described in the text.

the γ-decay scheme of these odd-even residual nuclei are more complicated than those of even-even nuclei. Also, we chose a bombarding energy range where the cross sections associated with these odd-even residual nuclei would usually be small.

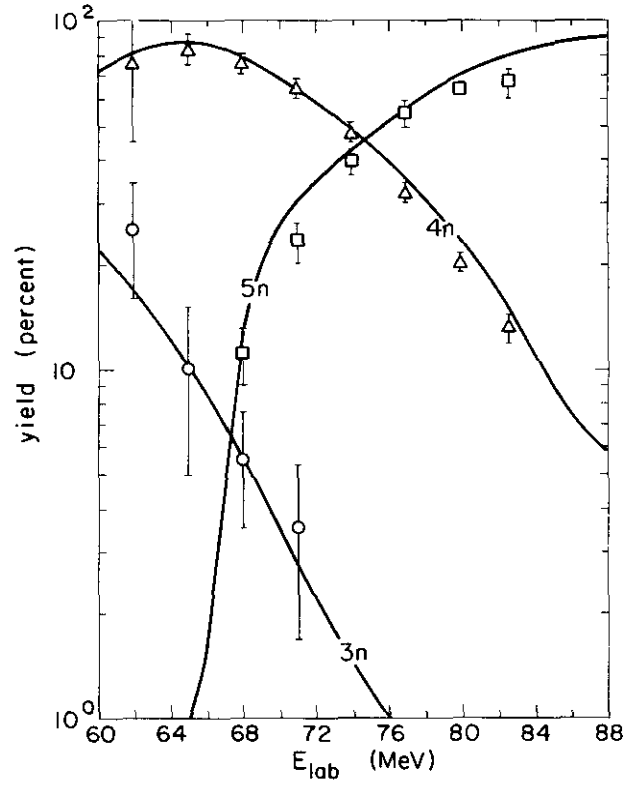

FIG. 3. Relative yields for the system $^{16}O+^{150}Nd$ as a function of the bombarding energy. The data points are from Ref. 12, whereas the solid curves are the predictions of CASCADE.

C. Determination of the fusion cross sections

In order to calculate the values of the fusion cross section σ_{fus} from the channel cross sections σ_{xn} it is necessary to know the relative yield $Y_{xn}=\sigma_{xn}/\sigma_{fus}$ for each energy. For the case of $\alpha+^{154}Sm$ and $^{12}C+^{154}Sm$ the values of Y_{xn} were not known, so that we have relied on the predictions given by the statistical decay code CASCADE (Ref. 6) for estimating Y_{xn}. The spin distributions required in these calculations have been obtained by iteration and are consistent with our final spin distributions. In order to assess the ability of this code for predicting Y_{xn}, we used

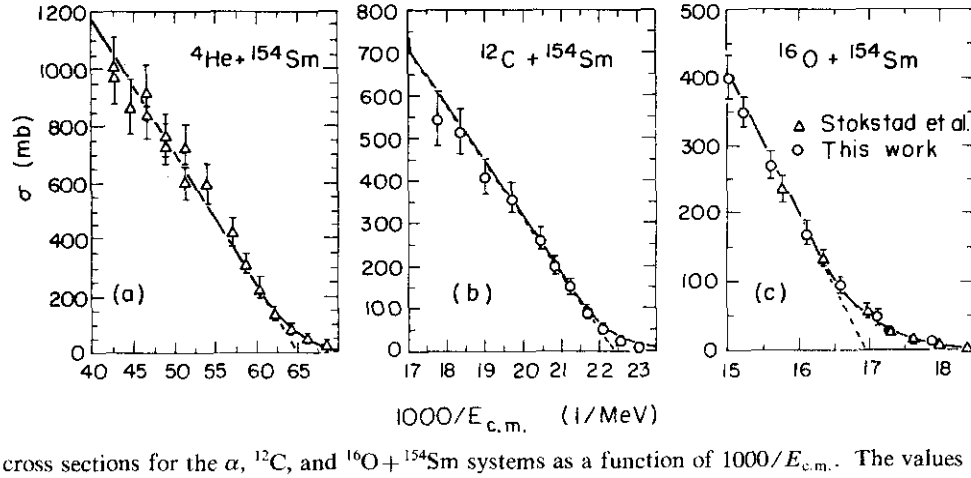

FIG. 4. Fusion cross sections for the α, ^{12}C, and $^{16}O+^{154}Sm$ systems as a function of $1000/E_{c.m.}$. The values of R_b and V_b were determined from the dotted straight line fitted to the above-barrier data using Eq. (13). The solid curve is the prediction of the Wong model using the parameters presented in Table III.

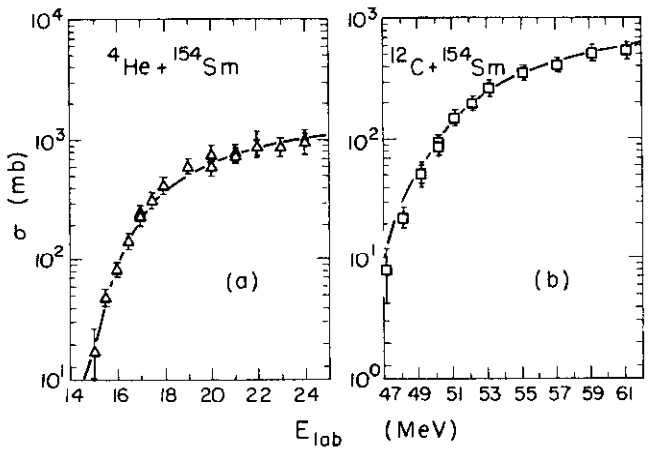

FIG. 5. Fusion cross sections for the α and $^{12}C+^{154}Sm$ system as a function of laboratory bombarding energy (E_{lab}). The solid curve represents the prediction of the Wong model using the parameters given in Table III.

the system $^{16}O+^{154}Sm$ as a test. Except for the characterization of the input spin distribution (see below) the default parameters of the code were generally employed. We found that the predictions of CASCADE agree quite nicely with the results obtained by Stokstad *et al.*[11]

For the case of $^{12}C+^{154}Sm$, we used the following semiempirical method. Since the reaction yields are experimentally known for the system $^{16}O+^{150}Nd$,[12] which leads to the same compound system as $^{12}C+^{154}Sm$ and in approximately the same region of excitation energy and angular momentum, we used the reaction $^{16}O+^{150}Nd$ as a bench mark for testing the predictions of the program CASCADE. The relative yields are also predicted quite well for this system, as shown in Fig. 3. This agreement indicates that the parameters used to obtain the decay of the CN are quite reasonable for calculating the relative yields; then maintaining the same parameters for the decay of the CN we use the code for calculating the Y_{4n} values for the case $^{12}C+^{154}Sm$. Since for a compound nuclear reaction one expects the decay of the CN to be independent of the way in which the CN was formed (except for the difference in angular momentum and excitation energy that the program CASCADE can account for), we expect that these predictions of Y_{4n} should be quite realistic.

In the case of $\alpha+^{154}Sm$, we have to rely entirely upon the prediction of the code CASCADE. By comparing the prediction of CASCADE with the experimental values we estimate an uncertainty of about 8% in the predicted value of Y_{xn}. In all the cases studied, the input spin distributions used in our CASCADE calculations were chosen iteratively so as to be consistent with the measured σ_{xn} and $\langle l \rangle$. The experimental results are displayed in Figs. 4 and 5.

IV. THEORETICAL MODELS: PRELIMINARY CONSIDERATIONS

A. A barrier-penetration model including target deformation effects

The fusion cross section can be written as

$$\sigma_{fus}(E)=\sum_l \sigma_l=\frac{\pi}{k^2}\sum_l (2l+1)P_l(E)\ , \tag{6}$$

where σ_l represents the partial fusion cross section, E and k are the c.m. bombarding energy and wave number for the relative motion, respectively. $P_l(E)$ represents the probability that a given partial wave l in the entrance channel leads to fusion. In the barrier penetration model one assumes that $P_l(E)$ is just equal to the penetrability of the effective interaction potential barrier.

A further simplification can be achieved, if we approximate the various effective interaction potentials around their relative maxima by inverted parabolas of height V_l and frequency ω_l. For a parabolic barrier the penetration coefficients $P_l(E)$ are given exactly by the Hill-Wheeler[13] formula

$$P_l(E)=\left\{1+\exp\left[2\pi\frac{(V_l-E)}{\hbar\omega_l}\right]\right\}^{-1}\ , \tag{7}$$

which is quantum mechanically correct for energies E both above and below V_l. The frequency ω_l depends on both the barrier curvature and the inertia parameter μ

$$\hbar\omega_l=\hbar\left\{\frac{1}{\mu}\left[\frac{\partial^2 V_{eff}(l,r)}{\partial r^2}\right]_{R_l}\right\}^{1/2}\ . \tag{8}$$

For commonly used potentials the values of R_l and $\hbar\omega$ are insensitive to l for the l values important in near-barrier fusion,[14,15] so that

$$R_l \simeq R_b = r_b(A_1^{1/3}+A_2^{1/3})\ , \tag{9}$$

$$\omega_l \simeq \omega\ , \tag{10}$$

where R_b, ω, and V_b represent the interaction radius, the frequency, and the barrier height for $l=0$, respectively.

If the characteristic time of the collision is short compared to the rotation time, the orientation of the target nucleus can be regarded as frozen throughout the collision. Esbensen *et al.*[16] have shown that the frozen approximation is quite good for collective excitations with $\hbar\omega \leq 1$ MeV. This criterion is readily satisfied for ^{154}Sm, which has a low lying 2^+ rotational state at $E_x=0.082$ MeV. If one denotes the angle between the symmetry axis of the deformed nucleus and the internuclear separation axis by θ, we can write for the height of the barrier

$$V_l(\theta)=V_{l=0}(\theta)+\frac{l(l+1)\hbar^2}{2\mu R_b^2}\ . \tag{11}$$

Consequently, according to Eq. (7), P_l now also depends on θ. The effective transmission coefficient $\langle P_l(E)\rangle$ can be obtained by averaging $P_l(\theta,E)$ over all possible orientations. In this manner we can write

$$\sigma_{fus}(E)=\langle\sigma_{fus}(E,\theta)\rangle$$

$$=\frac{\pi}{k^2}\sum_l (2l+1)\langle P_l(E,\theta)\rangle\ . \tag{12}$$

Equation (12) including quadrupole deformations was first developed by Wong.[14] It has been successfully applied to near barrier fusion by Scobel *et al.*[17] The computer code[18] that we have used in this work for calculating cross sections according to this model only takes into account the quadrupole deformation of the target nucleus; the projectile is regarded as spherical.

Before proceeding to a comparison of this one-dimensional barrier-penetration model including deformation with our results, we would like to briefly discuss some of the basic assumptions implicit in this model, and also to establish connections with some other models that have been developed for calculating fusion cross sections at sub-barrier energies.

Regarding the assumption of replacing the effective potential by an inverted parabola, we consider this to be a quite reasonable approximation. According to Eq. (7), the coefficients P_l are sensitive mostly to the potential in a rather narrow neighborhood around its maximum of width $\Delta E \simeq \hbar\omega/2$. Therefore as long as the second derivative of the effective potential does not vanish at its maximum and we are not dealing with energies far below the interaction barrier this assumption will be justified. For several commonly used nuclear potentials, Jahnke *et al.*[19] have found that $\hbar\omega \simeq 3 \pm 1$ MeV in the mass region under consideration. This assumes that the effective mass in Eq. (8) is equal to the reduced mass. The validity of this assumption for heavy targets is unclear at this time. Time-dependent Hartree-Fock calculations indicate that it is a reasonable approximation for $^{40}Ca+^{40}Ca$ but that for $^{12}C+^{12}C$ and $^{16}O+^{16}O$ there are significant increases in the inertial mass at internuclear separations corresponding to the top of the barrier.[20,21]

The above model can be generalized to include deformations other than quadrupolar, and to treat vibrational as well as rotational motion. Esbensen[22] has developed a simple model to account for the zero-point motion (ZPM) associated with the vibrational and rotational collective degrees of freedom. In this model, Esbensen assumes that the collective modes that are relevant are those for which the period of the collective motion is long as compared with the characteristic collision time. The rest of the modes only influence the relative motion in an average manner, and are included in the effective interaction potential. The relevant modes are treated within the impulse approximation, in a way similar to the Wong model, where the deformations are assumed to be frozen throughout the interaction, and l is assumed to be a good quantum number.[16] It should be emphasized that for the case of deformed nuclei, both the ZPM model and the Wong model contain basically the same physics and have similar limitations.

B. Coupled channels and optical models

More general formalisms that can accommodate the interaction between the relative motion and the intrinsic degrees of freedom have been developed, such as the coupled-channels formulation.[23] This useful generalization has been achieved at a great expense of simplicity. In our work we did not find it necessary to use this generalized treatment in order to obtain a reasonable account of our experimental results. The frozen-shape assumption of the simple models is particularly good for our case because of the well-developed rotational character of our target nucleus.

Finally, a model that has been extensively used for calculating elastic cross sections, reaction cross sections, and wave functions used as the starting point for more complex calculations, is the optical model. From this model it is possible to calculate the total amount of flux removed from the elastic channel which determines the total reaction cross section σ_R. Only when fusion is the dominant contributing channel is it justified to assume $\sigma_{\rm fus} \approx \sigma_R$. In spite of its ability to reproduce a wide variety of experimental results by properly adjusting the potential parameters, this model is more appropriate for calculating the angular dependence of the elastic cross section and determining the entrance channel wave functions than for understanding the relevant physical aspects of sub-barrier fusion. For instance, the enhancement of sub-barrier fusion cross sections observed in bombardment of several isotopes of Sm by ^{16}O, which increases with the deformation of the target,[11,24] can find a natural and simple explanation in the context of the Wong or the ZPM models by taking into account the enhancement in the fusion cross section introduced by the known deformations. The variation of the parameters of the optical potential necessary to obtain a good fit of the data would hardly convey the same physical insight into the problem.

V. INTERPRETATION OF EXPERIMENTAL RESULTS AND DISCUSSION

In this section we shall interpret our results for the fusion cross section and the first moment of the spin distribution by using a model that incorporates both barrier penetration and the averaging over the orientation of the deformed target.[14] We first discuss the results obtained for $\sigma_{\rm fus}$ as a function of the bombarding energy. From these data we deduce the model parameters V_b, r_b, and $\hbar\omega$ that are required to fit the data, and using the same parameters we then use the model for predicting the first moment of the spin distribution and compare these predictions with our experimental results.

A. Fusion cross sections

For bombarding energies above the Coulomb barrier the fusion cross section is given by

$$\sigma_{\rm fus}(E) \simeq \pi R_b^2 \left[1 - \frac{V_b}{E} \right] . \tag{13}$$

Thus one expects a linear dependence of the fusion cross section with the inverse of the center of mass energy. Consequently from the slope and the interaction of a line fit to the data in such a plot, it is possible to determine values of the interaction radius R_b and the interaction barrier V_b.

In Fig. 4 we present our data of $\sigma_{\rm fus}$ vs $1000/E_{\rm c.m.}$ for the cases of α, ^{12}C, and ^{16}O on ^{154}Sm, respectively. From these figures, it is clear that the high energy data indeed show a linear behavior in this representation. From the dotted straight lines we extracted the values of R_b and V_b for each system studied. In Table III we present the values of these parameters for each case.

The values of $\hbar\omega$ were determined from the experimental fusion cross sections at energies less than and about that of the interaction barrier. This is the same region in which the nuclear deformation also affects the behavior of the $\sigma_{\rm fus}$, so it is not possible from the fusion cross section

TABLE III. Barrier penetration model parameters. Typical uncertainties in r_b and V_b are 3% and 5%, respectively.

System	r_b (fm)	V_b (MeV)	β	$\hbar\omega$ (MeV)
$\alpha+{}^{154}$Sm	1.42	15.4	0.22	2.4
^{12}C$+{}^{154}$Sm	1.26	44.6	0.22	2.0
^{16}O$+{}^{154}$Sm	1.35	59.0	0.22	3.5
^{40}Ar$+{}^{154}$Sm	1.35	128.0	0.22	4.9

data alone to determine both $\hbar\omega$ and the deformation parameter β, as will be discussed in more detail later.

Quantitative information on the quadrupole deformation, characterized by the parameter β, has been obtained by several independent methods[25] such as α-particle scattering[23,26] electromagnetic transitions in μ-mesic atoms,[27] and from reduced $E2$ transition matrix elements, $B(E2,2\rightarrow 0)$.[28] Even though there are some discrepancies in the values obtained for β among the different methods,[25] all these methods yield values of β between 0.2 and 0.3. We have been able to obtain a good fit of the fusion cross sections for all the systems studied using $\beta=0.22$ for ^{154}Sm and assuming a spherical shape for the projectiles. Additional support for using this particular value for the deformation of ^{154}Sm is the fact that with this same value of β it has been possible to achieve quite a nice fit[2] of the ^{40}Ar$+{}^{154}$Sm data using a value of $\hbar\omega=4.9$ MeV.

It is also important to notice that $\hbar\omega$ cannot be regarded as a completely free parameter. Its value, in order to be physically meaningful, has to agree with the values one would obtain by using some of the well-tested nuclear potentials.[29] The values of $\hbar\omega$ that were required for obtaining the fits depicted in Fig. 2 are presented in Table II and for the systems studied here are in the expected range[19] of $\hbar\omega\approx 3\pm 1$ MeV.

The values of $\hbar\omega$ obtained for ^{12}C and α, although consistent with *a priori* expectations, should be taken with some caution, particularly for the case of ^{12}C. As we have seen previously, the fusion cross section data that are relevant for determining $\hbar\omega$ are the near- and sub-barrier data, which in our particular case have the largest errors. In particular we suspect that in the case of ^{12}C the low energy data for the fusion cross section may have been overestimated due to the fact that the code CASCADE (Ref. 6) has shown a tendency to overpredict the (HI,4n) yield at lower energies.

B. Average angular momentum of the spin distributions

Using the barrier-penetration model including deformation and the same parameters used for fitting the fusion cross sections (see Table III) we calculated the first moment of the spin distribution as a function of energy. The results of these calculations and the values of $\langle l\rangle$ obtained from our experiments, as described in the previous section, are depicted in Fig. 6 for the cases of α, ^{12}C, and ^{16}O on ^{154}Sm. In all these plots the error bars on the data include both the uncertainties in the measured multiplicities as well as the uncertainties in converting them to angular momentum as was discussed previously. The model used is in good agreement with the results obtained in the present experiment as well as the earlier results on ^{16}O$+{}^{154}$Sm.

For the case of $\alpha+{}^{154}$Sm (Fig. 6) we see that the sharp cutoff expectations for the average angular momentum $\langle l\rangle$ seem to reproduce the results quite well. This fact may be associated with the manner in which Eq. (2) was obtained, namely by comparing the measured γ multiplicities at bombarding energies well above the barrier in reactions using light ions (e.g., α particles) with the values of $\langle L\rangle$ obtained using the sharp cutoff estimates. Therefore, the sharp cutoff expectations for the case of $\alpha+{}^{154}$Sm [Figs. 6 and 11(a)] show the self-consistency of Eq. (2) for relating average angular momentum with γ multiplicities.

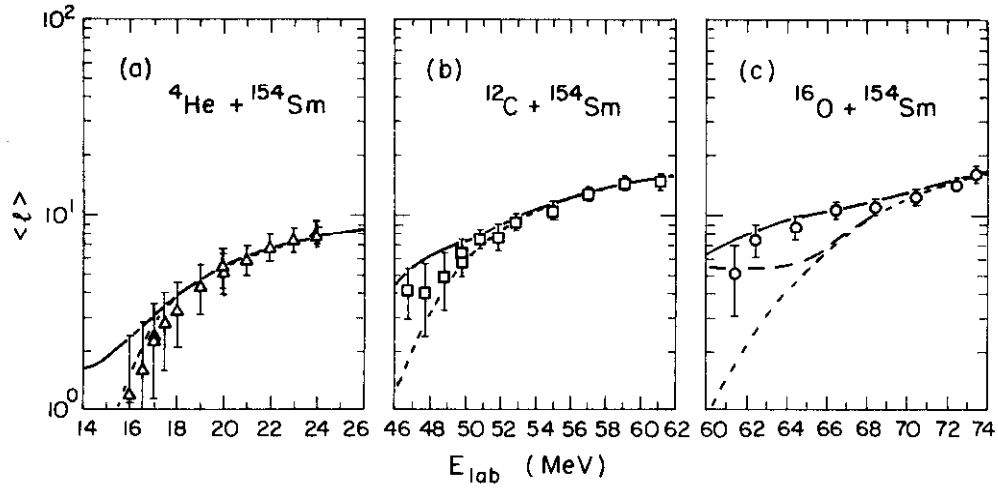

FIG. 6. Average angular momentum of the spin distribution in the compound nucleus produced in the ^{4}He, ^{12}C, and ^{16}O$+{}^{154}$Sm reactions. The solid curve is the prediction of $\langle l\rangle$ obtained using the Wong model with the parameters given in Table III. The short-dashed curve represents the expectation of $\langle l\rangle$ according to the sharp cutoff model, namely, $\langle l\rangle=l_{crit}/1.5$, where the values of l_{crit} were obtained from the experimental fusion cross sections. The long-dashed curve in (c) is the prediction of the Wong model when the target deformation is neglected, i.e., $\beta=0$.

C. Spin distribution of the compound nucleus

In Figs. 7–9 we show the results of our model for the spin distribution for α, ^{12}C, and ^{16}O on ^{154}Sm, respectively, for two bombarding energies above and below the Coulomb barrier for each case. Also in the same figures we show for comparison, by dotted lines, the expectation for the spin distribution according to the sharp cutoff model. As can be noticed from these figures, the sharp cutoff prescription for determining the first moment of the spin distribution of the CN becomes progressively worse as we go to energies below the Coulomb barrier. Note also that the l_{crit} values for the sharp cutoff model already include the lowest order effects of barrier penetration in enhancing the fusion cross section, in that l_{crit} has been deduced from the experimental cross section. In particular at energies below the Coulomb barrier, these figures suggest that the spin distributions are much broader than what one would expect from the sharp cutoff model.

At higher bombarding energies the sharp cutoff gives a fair approximation of the spin distribution. In particular, for the first moment of the spin distribution at energies well above the Coulomb barrier, the experimental data agree with both the prediction of our model as well as the values obtained using the sharp cutoff prescription. Figure 6(c) clearly illustrates this point. Although the mean spin values (first moments) of the realistic and the sharp cutoff distributions become similar at high energies, the distributions have significant differences as revealed by the higher moments of the distributions.

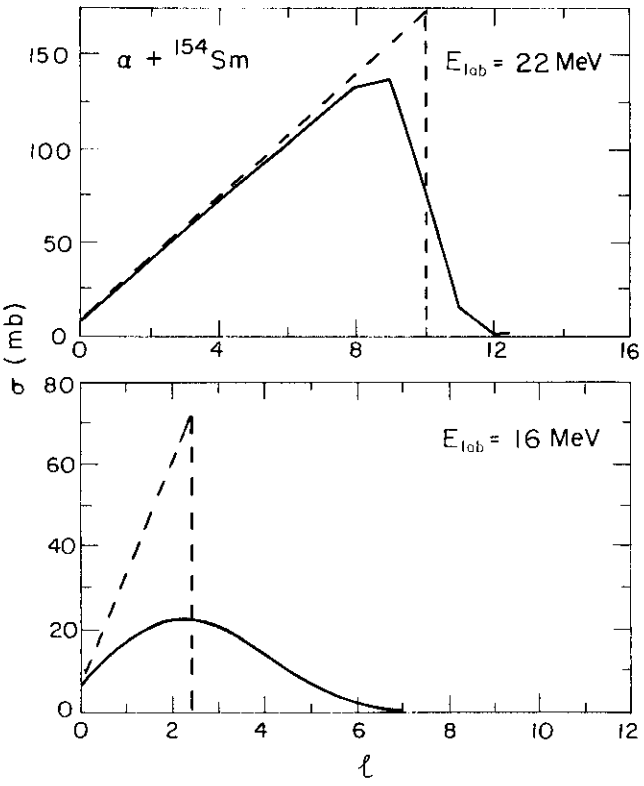

FIG. 7. Comparison of the spin distributions obtained using the Wong model (solid curves), and the same distributions obtained using the sharp cutoff prescription (dashed lines), for the compound nucleus produced in the reaction $\alpha+^{154}Sm$, at the laboratory energies indicated in the figures. The Coulomb barrier for this system is $V_b \simeq 16$ MeV in the laboratory system.

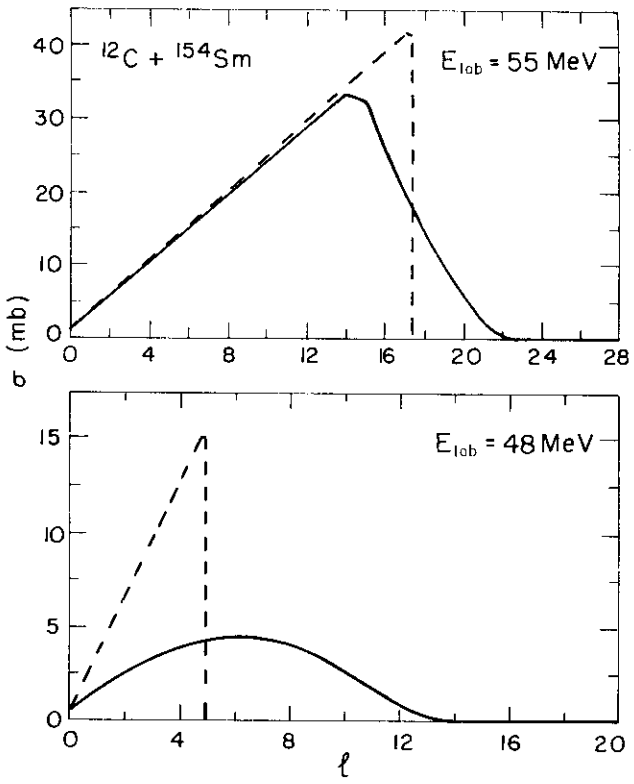

FIG. 8. Comparison of the spin distributions obtained using the Wong model (solid curves), and the same distributions obtained using the sharp cutoff prescription (dashed lines), for the compound nucleus produced in the reaction $^{12}C+^{154}Sm$, at the laboratory energies indicated in the figures. The Coulomb barrier for this system is $V_b \simeq 48$ MeV in the laboratory system.

Another important characteristic to be noticed in these figures is the fact that the discrepancy between the model used and the sharp cutoff prescription increases with the mass of the projectile. In order to gain some insight into the physical reason behind this difference between the Wong model and the sharp cutoff prescription, let us recall the physical assumptions underlying the two models.

In the sharp cutoff model one implicitly neglects the quantum mechanical penetration effects, i.e., one assumes that at a given bombarding energy the probability of penetrating the effective interaction barrier is unity for all partial waves below a certain l_{crit} and is zero for the rest of the partial waves, that is, $P_l=1$ for $l \leq l_{crit}$ and $P_l=0$ for $l > l_{crit}$, so that using Eq. (6) we have

$$\sigma_{fus}=\frac{\pi}{k^2} l_{crit}(l_{crit}+1) . \tag{14}$$

Within this model l_{crit} would represent the number of partial waves that are required to be removed from the elastic channel in order to obtain the experimental fusion cross section. According to the sharp cutoff model one would also have $l_{crit}=1.5\langle l \rangle$, corresponding to a triangular distribution that would be expected in this case. Also in this model, by assuming a step function for the coefficients P_l, one neglects the quantum mechanical aspects of the penetration through the barrier and reflection above

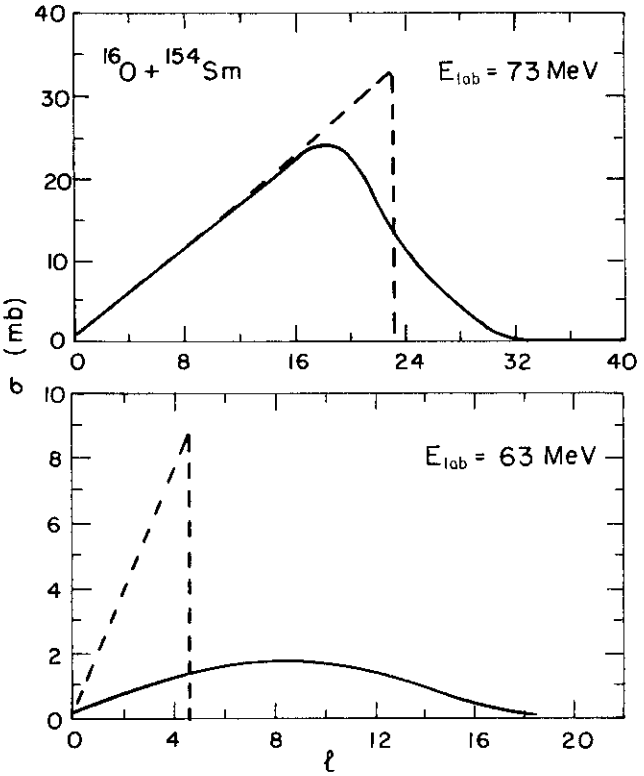

FIG. 9. Comparison of the spin distributions obtained using the Wong model (solid curves), and the same distributions obtained using the sharp cutoff prescription (dashed lines), for the compound nucleus produced in the reaction $^{16}O+^{154}Sm$, at the laboratory energies indicated in the figures. The Coulomb barrier for this system is $V_b \simeq 65$ MeV in the laboratory system.

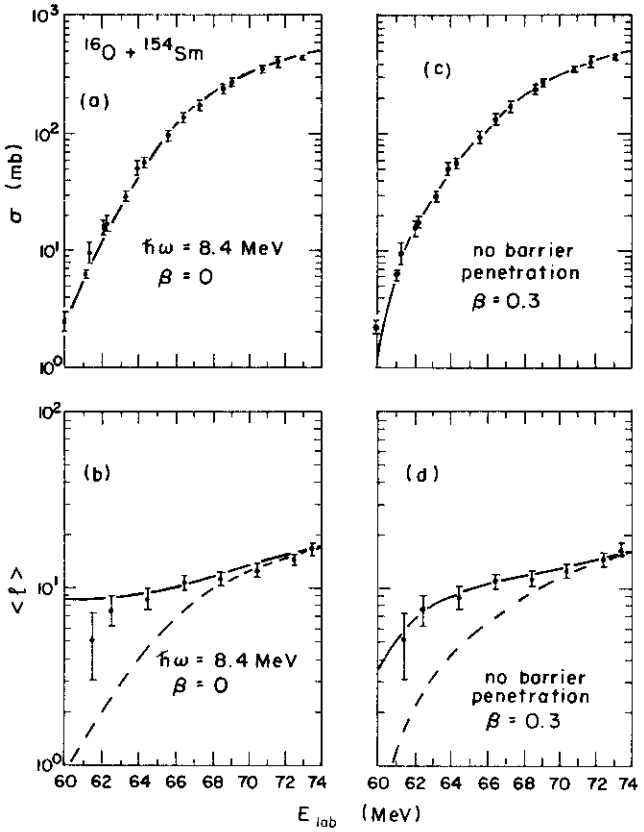

FIG. 10. Fusion cross sections and average angular momentum of the spin distribution for the system $^{16}O+^{154}Sm$. The fits to the data was obtained using the Wong model with the values of $\hbar\omega$ and β indicated in the figures. These values of $\hbar\omega$ and β represent two extreme but equally unphysical situations. When no barrier penetration is allowed, the smearing of the coefficient P_l is generated by an exaggerated target deformation. In the case of $\beta=0$, the smearing is caused by an unrealistically penetrable barrier. The dashed curves in (b) and (d) are the values obtained from the sharp cutoff prescription.

the barrier as well as any other effect that may cause a smearing of the coefficients P_l around l_{crit}, such as target or projectile deformation.

In the barrier penetration model, due to the interplay of the quantum mechanical barrier penetration, determined in this model by $\hbar\omega$, and the effects of the quadrupole deformation of the target represented by the parameter β, it is possible to compensate the variation of one of these parameters ($\hbar\omega$ or β) by an appropriate change in the other. In Fig. 10 we have tried to illustrate this point by presenting a set of fair fits to the experimental data, for the case of $^{16}O+^{154}Sm$, using two extreme but equally unphysical values for the parameters $\hbar\omega$ and β. Although a reasonable fit can be obtained using $\beta=0$ and $\hbar\omega=8.4$ MeV, neither of these values is consistent with what is known for this system. Similarly the calculation with no barrier penetration ($\hbar\omega\rightarrow 0$) is completely unphysical and in disagreement with what is known about the potential. For this reason it is important when using this model to examine the consistency of these parameters with other sources of information. The long-dashed curve in Fig. 6(c) shows the effect of neglecting the effect of target deformation while keeping a realistic shape of the barrier. From this comparison we conclude it is necessary to include both barrier penetration and target deformation effects. The important role of deformation in determining the total fusion cross section at sub-barrier energies has been established in studies[11,24] of the fusion cross sections for different Sm isotopes, which vary from nearly spherical nuclei to quite deformed nuclei.

D. Comparison among the different systems studied

If the deformation degrees of freedom are constant among the different systems studied, which in the present work is approximately achieved by using always the same target, the differences in the spin distribution of the CN produced in each of the reactions used arise from the variation in the angular momentum dependent part of the effective potential.

Furthermore, at the effective interaction distance R_b where V_{eff} reaches its maximum value, we have the condition

$$\frac{\partial V_{eff}}{\partial l} = \frac{(2l+1)\hbar^2}{2\mu R_b^2} . \tag{15}$$

As the mass of the projectile changes, μ and R_b vary. For the case of α, ^{12}C, and ^{16}O on ^{154}Sm, the values of μR_b^2 are in the ratio of 1:3.5:5, respectively. In the language of the barrier-penetration model, this means that for heavier

projectiles more partial waves have barriers comparable to the incident energy and can be affected by barrier penetration and reflection. This will lead to relatively broader spin distributions for heavier projectiles.

In Fig. 11 we present our experimental $\langle l \rangle$ values for the different projectiles α, ^{12}C, and ^{16}O. We use l_{crit}, obtained from the experimental values of σ_{fus} using Eq. (14), as a convenient scaling parameter. The straight line $l_{crit} = 1.5\langle l \rangle$, that would be the expected relationship between these two quantities according to the sharp cutoff prescription, is also shown in this figure for reference.

Our results clearly display the expected behavior, namely that the larger the mass of the projectile the larger the deviation from the extreme sharp cutoff model for a given value of l_{crit}, and consequently the broader the spin distribution for this system. Also we see that as the energy (and l_{crit}) increases, the relation between $\langle l \rangle$ and l_{crit} tends to approach that of the sharp cutoff model. In Figs. 11(b), (c), and (d) we present, in the same representation, the results corresponding to the cases of α, ^{12}C, and ^{16}O on ^{154}Sm, together with the prediction obtained using the barrier-penetration model including deformation. The error bars in $\langle l \rangle$ now include both the uncertainties in the measured multiplicities and the uncertainties in converting them to angular momentum as discussed before.

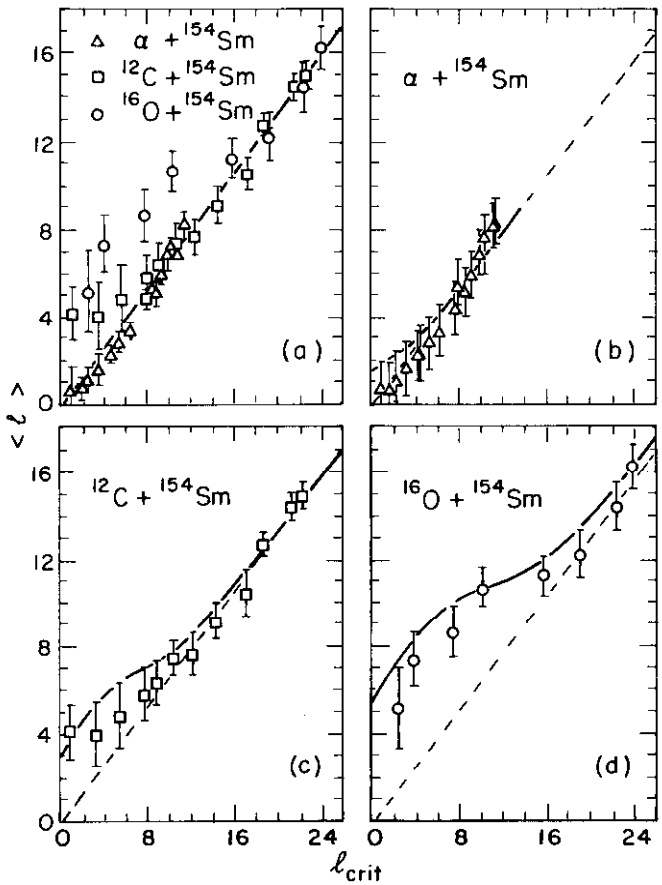

FIG. 11. Experimental values of $\langle l \rangle$ plotted versus l_{crit}. The values of $\langle l \rangle$ were obtained from the measured gamma multiplicities using Eq. (2) whereas the corresponding values of l_{crit} were obtained from the fusion cross sections using Eq. (14). The error bars in this figure only include the statistical errors in $\langle l \rangle$. In (b), (c), and (d) we show values for the different systems, separately. The error bars of $\langle l \rangle$ now include both the uncertainties in the measured multiplicities as well as the uncertainties in converting them to angular momentum. The solid curves are the predictions of the Wong model for these systems.

VI. CONCLUSIONS

We have measured the gamma multiplicity M_γ, and the cross section for the dominant reaction channel for the systems $\alpha + ^{154}$Sm and ^{12}C + ^{154}Sm at near-barrier bombarding energies. Our main objective was to obtain information about the spin distribution of the compound nucleus produced in these reactions and to gain some insight to the physical features that determine the deviation of this spin distribution from simple sharp cutoff estimates. In particular, by using different projectiles on the same target we have varied the reduced mass of the system while maintaining a constant target deformation, enabling us to address the question of how relevant the centrifugal potential penetrability is in determining the spin distribution of the CN.

One of the most interesting aspects of our study is the striking difference in the bombarding energy dependence of the fusion cross section and the gamma multiplicity. While the first varies in each of the systems studied by about three orders of magnitude over the bombarding energy range studied here, the gamma multiplicities show a much slower variation in the same bombarding energy interval.

In order to characterize the spin distribution of the CN we have used as a reference a triangular distribution and we have analyzed the deviations from this shape that were inferred from our experimental results. We found that at high energies the sharp cutoff is a reasonable approximation. More specifically, the values of $\langle l \rangle$ obtained from the shape cutoff model using Eq. (14) together with $l_{crit} = 1.5\langle l \rangle$ are consistent with our experimental results at energies well above the Coulomb barrier (see Fig. 6).

At energies near and below the Coulomb barrier we found that the predictions of the sharp cutoff model for $\langle l \rangle$ start to underestimate our experimental results, with the discrepancy larger for the more massive projectiles. At these energies our data for $\langle l \rangle$ indicate a much broader spin distribution than the one that would be expected from the sharp cutoff model, especially for cases of heavier projectiles (larger reduced mass). Figures 7–9 indicate how inadequate the spin distributions predicted using the sharp cutoff model can be at these low bombarding energies.

The broad spin distributions that we found at subbarrier energies can be accounted for if we take into account both the penetrability of the centrifugal potential, and the effects of target deformation. The different behavior exhibited by the different systems [see Fig. 11(a)] clearly indicates the relevance of the centrifugal barrier penetrability in determining the spin distribution of the CN, since in all the systems studied we used the same target, and therefore the contribution of the deformation to the broadening is supposed to be constant. The difference in the broadening of the spin distribution can be easily understood by noting that for heavier projectiles (large μR_b^2),

according to Eq. (15), the effective interaction barriers have a slower variation with l; in other words, the effective potential does not change much from one l to the next. Therefore the penetrability coefficients P_l also have a smoother variation with l for the more massive projectiles and consequently the spin distributions are broader.

Inclusion of barrier penetration effects alone does not adequately account for the observed $\langle l \rangle$ values, as can be seen by comparison of the dashed line with the experimental data. It is necessary to include the deformation effects to understand both the absolute value of the fusion cross sections at sub-barrier energies and the absolute value of $\langle l \rangle$ at near-barrier energies. The one-dimensional barrier-penetration model including deformation, as developed by Wong,[14] can account for the experimental results very nicely. Equivalent approaches, such as the ZPM model,[22] can also reproduce the experimental results.[2] The success of these models together with their simplicity make these models very useful for predicting spin distributions in this mass region. For all these systems we have found it unnecessary to appeal to the inclusion of additional degrees of freedom.

The degree of agreement between our experimental results and the prediction of the barrier-penetration model including deformation also suggests that the assumption made of regarding the inertia parameter μ as the reduced mass of the entrance channel is adequate in these cases. Moreover, the variation of the reduced mass of the entrance channel accounts very well for the variation found in the behavior of the different systems used in this work.

This work was supported in part by the U. S. Department of Energy.

*On leave of absence from Comision Nacional de Energia Atomica, Buenos Aires, Argentina while this work was in progress.

[1]C. Brun, B. Gatty, M. Lefort, and X. Tarrago, Nucl. Phys. **A116**, 117 (1968).

[2]R. Vandenbosch, B. B. Back, S. Gil, A. Lazzarini, and A. Ray, Phys. Rev. C **28**, 1161 (1983).

[3]V. Metag *et al.*, in Proceedings of the INS-RIKEN International Symposium on Heavy Ion Physics, Part II, Mt. Fuji, Japan, edited by S. Kubono, M. Ishihara, and M. Ichimura, J. Phys. Soc. Jpn. Suppl. **54**, 439 (1985).

[4]B. B. Back, R. R. Betts, K. Cassidy, B. G. Glagola, J. E. Gindler, L. E. Glendenin, and B. D. Wilkins, Phys. Rev. Lett. **50**, 818 (1983).

[5]M. B. Tsang, H. Utsonomiya, C. K. Gelbke, W. G. Lynch, B. B. Back, S. Saini, P. A. Baisden, and M. A. McMahon, Phys. Lett. **129**, 18 (1983).

[6]F. Puhlhofer, Nucl. Phys. **A280**, 267 (1977).

[7]*Table of Isotopes*, 7th ed., edited by C. M. Lederer and V. S. Shirley (Wiley, New York, 1978).

[8]G. B. Hagemann, R. Broda, B. Herskind, M. Ishihara, S. Ogaza, and H. Ryde, Nucl. Phys. **A245**, 166 (1975).

[9]S. H. Sie, J. O. Newton, and J. R. Leigh, Nucl. Phys. **A245**, 279 (1981).

[10]M. N. Namboodiri, J. B. Natowitz, P. Kasiraj, R. Eggers, L. Adler, P. Gonthier, C. Cerruti, and S. Simon, Phys. Rev. C **20**, 982 (1979).

[11]R. G. Stokstad, Y. Eisen, S. Kaplanis, D. Pelte, U. Smilansky, and I. Tserruya, Phys. Rev. C **21**, 2427 (1980).

[12]R. Broda, M. Ishihara, B. Herskind, H. Oeschler, S. Ogaza, and H. Ryde, Nucl. Phys. **A248**, 356 (1975).

[13]D. L. Hill and J. A. Wheeler, Phys. Rev. **89**, 1102 (1953).

[14]C.-Y. Wong, Phys. Rev. Lett. **31**, 766 (1973).

[15]D. Glas and U. Mosel, Nucl. Phys. **A237**, 429 (1975).

[16]H. Esbensen, J.-Q. Wu, and G. F. Bertsch, Nucl. Phys. **A411**, 275 (1983).

[17]W. Scobel, A. Mignery, M. Blann, and H. H. Gutbrod, Phys. Rev. C **11**, 1701 (1975).

[18]B. B. Back, private communication.

[19]U. Jahnke, H. H. Rossner, D. Hilscher, and E. Holub, Phys. Rev. Lett. **48**, 17 (1982).

[20]H. Flocard, P. H. Heenen, and D. Vautherin, Nucl. Phys. **A339**, 336 (1980).

[21]P. H. Heenen, H. Flocard, and D. Vautherin, Nucl. Phys. **A344**, 525 (1983).

[22]H. Esbensen, Nucl. Phys. **A352**, 147 (1981).

[23]N. K. Glendenning, *Direct Nuclear Reactions* (Academic, New York, 1983).

[24]W. Reisdorf, F. P. Hessberger, K. D. Hildenbrand, S. Hofmann, G. Munzenberg, K.-H. Schmidt, J. H. Schneider, W. F. W. Schneider, K. Summerer, and G. Wirth, Phys. Rev. Lett. **49**, 1811 (1982).

[25]R. G. Stokstad and E. E. Gross, Phys. Rev. C **23**, 281 (1981).

[26]D. L. Hendrie, N. K. Glendenning, B. G. Harvey, O. N. Jarvis, H. H. Duhm, J. Saudinos, and J. Mahoney, Phys. Lett. **26B**, 127 (1968).

[27]P. M. Endt and C. Van der Leun, Nucl. Phys. **A214**, 1 (1973).

[28]P. H. Stelson and L. Grodzins, Nucl. Data Sect. **A1**, 21 (1965).

[29]H. J. Krappe, K. Mohring, M. C. Nemes, and H. Rossner, Z. Phys. A **314**, 23 (1983).